Spiral Waves in Liquid Crystal

T. Frisch, S. Rica, P. Coullet, and J. M. Gilli*
Institut non-Linéaire de Nice, Unité Mixte de Recherche CNRS 129, 1361 Rt. des Lucioles, 06560 Valbonne, France
(Received 20 September 1993)

We report experimental investigation and theoretical interpretation of the formation of spiral waves in a nematic liquid crystal subjected to a rotating magnetic field and a high frequency electrical field.

PACS numbers: 47.20.Ky, 61.30.Gd, 61.30.Jf

The application of a magnetic field on nematic liquid crystal leads to the formation of walls [1]. These walls separate domains of different orientation of the molecules. It is reported in [2–4] the spontaneous transformation of some of these domains walls into moving walls and spiral waves. We shall refer to the wall described in [2,3] as the Brochard-Leger (BL) wall. In [4] the qualitative description of the structural transition of the BL wall into the moving wall was given. In this Letter, we present experimental results which report a transition of the BL wall and the formation of spiral waves comparable to the ones described in [4]. Furthermore, we derive a theoretical quantitative model from the nematic elasticity theory which falls in good agreement with the experimental results. In particular, we will interpret the transition of the BL walls to moving walls as a nonequilibrium Ising-Bloch (IB) transition [5]. Similar ideas have been applied to reaction-diffusion systems [6] in which domain walls and spiral waves are also observed.

The experiment (Fig. 1) consists of a nematic liquid crystal sandwiched between two glass plates in a homeotropic geometry (molecules perpendicular to the glass plates) subjected to a magnetic field H parallel to the plates and an electric field perpendicular to them. The magnetic field can be either fixed or rotating in the (x, y) plane at a frequency ω around an axis perpendicular to the plate while the electric field E parallel to the z axis oscillates at high frequency in order to avoid convection effects. A motor rotates a plate at a frequency ω supporting two small permanent Nd-Fe-B magnets, which produce a magnetic field of 0.5 T between the poles. The homeotropic anchoring is achieved by treating our glass plates with lecithin. The thickness d of the sample was in general about 75 μm. The liquid crystal used is MBBA, nematic at room temperature with negative dielectric anisotropy. More experimental details can be found in [7].

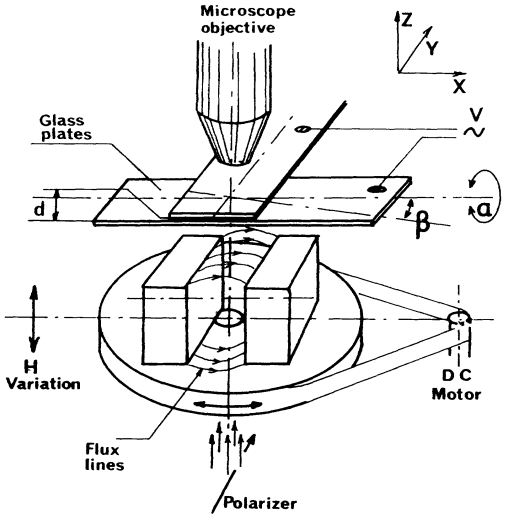

FIG. 1. Scheme of the experiment. The ITO treated glass plates filled with homeotropic nematic are positioned in the air-gap upper region of a high flux permanent magnet allowed to rotate around the polarizing microscope axis. The magnetic field is varied by the adjusment of the distance between the nematic slab and the upper surface of the magnets.

The experiment of [4] reports several striking results as the main parameters of the experiment; the intensity of the magnetic field and the frequency of rotation are varied. Stationary BL are transformed into moving solitons when ω is increased beyond a certain range. Two-arm spiral waves are found to be stable in a large parameter space. The core of these spiral waves is an umbilic of topological charges $+1$ or -1. The wave number of the $+1$ spiral wave is different from the wave number of the -1 umbilic. As a result the spiral with the larger wave number takes over the one with the smaller wave number.

We report the observation of two-arm spiral waves (Fig. 2) and also the observation of an Ising-Bloch transition of the BL wall with a stationary or rotating magnetic field as the intensity of the electrical field is varied. The originality of our experiment is in the use of molecules with a negative dielectric anisotropy so that the homeotropic state can be destabilized by the application of the electrical field. As a consequence, we can operate in the vicinity of the Freedericksz [8] transition: This enables us to do a weakly nonlinear analysis of the transition.

When a stationary horizontal magnetic field is applied to the sample, the nematic director tends to align along the field direction. Because of the homeotropic boundary conditions which impose the initial vertical alignment, an elastic restoring torque is also present. The balance between these two effects defines the onset of the Freed-

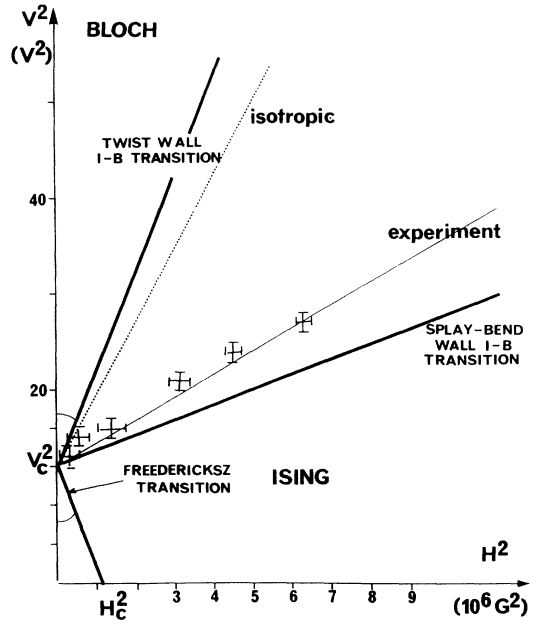

FIG. 2. The experimental and theoretical phase diagram of the static Ising-Bloch transition ($\omega = 0$) in the (V^2, H^2) parameter space with $V = dE$. The dark lines have been obtained using Eq. (2). The light grey line has been obtained experimentally using the setup of Fig. 1.

ericksz transition. The order parameter for these experiments is the projection of the director on the (x, y) plane. Above the threshold of the Freedericksz transition, BL walls [2,3] in which the director points along the z axis appear. In analogy with ferromagnetic systems [9,10], we shall refer to BL walls as Ising walls, since the order parameter vanishes at the center of the wall. To be consistent with this previous definition, walls in which the director is never pointed along the z will be referred to as Bloch walls. The effect of the electrical field used in [7] is to induce an Ising-Bloch transition of the BL wall. Such a transition is produced by the effect of the electrical field, which forces the molecules to reorient toward a plane perpendicular to the z axis. In Fig. 2 we show an experimental measurement of the IB transition for a BL wall.

As yet understood in terms of general argument in [5] and qualitative argument in [4], the effect of the rotation is to induce a movement of the Bloch wall. Bloch walls may be connected by a line (umbilic line) in which the director points towards the z axis. This configuration naturally evolves into a spiral wave when subjected to a rotating magnetic field. We show in Fig. 3 a photograph of a spiral wave obtained using the experimental setup described in Fig. 1.

Our theoretical approach assumes that the director is only weakly tilted from the z axis. This condition is fulfilled only in the vicinity of the Freedericksz transition,

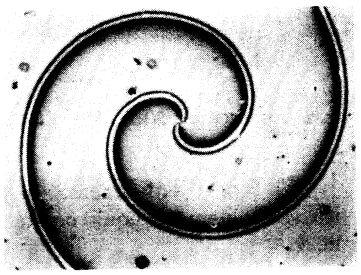

FIG. 3. Photograph of a spiral obtained with the setup of Fig. 1 in the parameter region corresponding to region C of Fig. 4.

a condition which is not fulfilled in [4]. In this condition it is legitimate to neglect backflow effects. Furthermore, the magnetic field is considered as a small perturbation of the main electrical field. The dynamical equation for the director, $\mathbf{n}$, reads [8]

$$\gamma_1 \mathbf{n} \times \mathbf{n}_t = -\mathbf{n} \times \frac{\delta F}{\partial \mathbf{n}}, \tag{1}$$

where γ_1 is the rotational viscosity and the Frank free energy reads

$$F = \frac{1}{2}\int dv[K_1(\boldsymbol{\nabla}\cdot\mathbf{n})^2 + K_2(\mathbf{n}\cdot\boldsymbol{\nabla}\times\mathbf{n})^2 + K_3(\mathbf{n}\times\boldsymbol{\nabla}\times\mathbf{n})^2 - \chi_a(\mathbf{H}\cdot\mathbf{n})^2 - \epsilon_a(\mathbf{E}\cdot\mathbf{n})^2],$$

where $\mathbf{H} = H[\cos(\omega t)\hat{\mathbf{x}} - \sin(\omega t)\hat{\mathbf{y}}]$, $\mathbf{E} = E\hat{\mathbf{z}}$, and K_1, K_2, K_3 are the elastic constants. The linear stability analysis of Eq. (1) reveals that when $E > E_c$, which will be defined later, the homeotropic state $\mathbf{n} = \hat{\mathbf{z}}$ becomes unstable.

It is then natural to make a vertical Fourier expansion in which we retain only the first unstable mode. It can easily be shown that in the vicinity of the Freedericksz transition the higher order vertical distortion modes are damped and therefore follow adiabatically the first unstable mode. Let us choose for an order parameter, $A(x, y) = X(x, y) + iY(x, y)$, which measures the deviation from the homeotropic state, where $X(x, y)$ and $Y(x, y)$ are defined by $n_x = X(x, y)\cos(\frac{\pi}{d}z)$,

$$n_y = Y(x,y)\cos\left(\frac{\pi}{d}z\right), \quad n_z = 1 - \frac{n_x^2 + n_y^2}{2},$$

and d is the thickness of the sample. Direct replacement of this ansatz into Eq. (1) leads after some algebra to

$$\gamma_1 A_t = \mu A + \gamma \bar{A} e^{-2i\omega t} + \frac{K_1 + K_2}{2}\nabla^2 A + \frac{K_1 - K_2}{2}\bar{A}_{\eta\eta} - a|A|^2 A, \tag{2}$$

where $\eta = x - iy$, $\nabla^2 = \partial_{xx} + \partial_{yy} = \partial_\eta \partial_{\bar{\eta}}$, $\partial_\eta = \partial_x + i\partial_y$, $\mu = \frac{\chi_a}{2}H^2 - \epsilon_a E^2 - K_3\frac{\pi^2}{d^2}$, $\gamma = \frac{\chi_a}{2}H^2$, $a = \frac{1}{2}(K_1 -$

$\frac{3}{2}K_3)\frac{\pi^2}{d^2} - \frac{3}{4}\epsilon_a E^2$, and $\bar{A}$ stands for the complex conjugate. This equation is very similar to the one studied in [5] except for the term $\bar{A}_{\eta\eta}$, which is proportional to the anisotropy of elasticity $(K_1 - K_2)$.

For simplicity, we first discuss the case $K_1 = K_2$. Equation (2) simplifies after the transformation $A \to Ae^{-i\omega t}$ to

$$\gamma_1 A_t = (\mu + i\gamma_1\omega)A + \gamma\bar{A} + K_1\nabla^2 A - a|A|^2 A. \quad (3)$$

Let us take E to be slightly smaller than $E_c = \sqrt{\frac{K_3\pi^2}{-\epsilon_a d^2}}$. Note that the dielectric anisotropy ϵ_a is negative. The linear stability analysis of Eq. (3) yields that the homeotropic state $A = 0$ loses stability when $H > H_1(\omega, E)$ (Fig. 4).

Let us now place ourselves in the synchronous region (Fig. 4) in which the director rotates at the same frequency as the magnetic field ($\omega < \frac{\chi_a H^2}{2\gamma_1}$). In this region there exist two stable homogeneous solutions of Eq. (3) which read $A = \pm\sqrt{\frac{\mu+\gamma\cos 2\delta}{a}}e^{i\delta}$ where δ is defined by

$$\sin(2\delta) = \frac{\gamma_1\omega}{\gamma}.$$

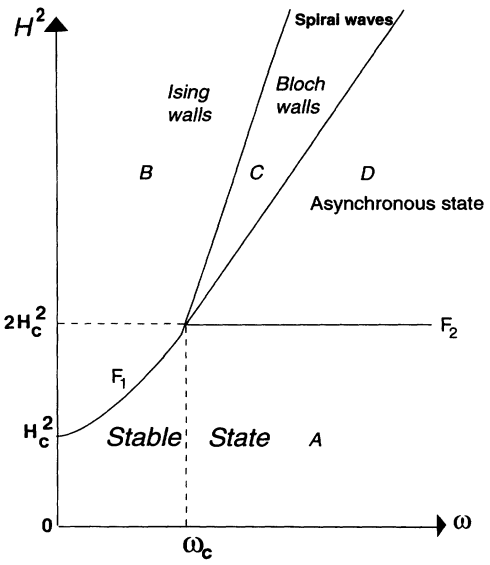

FIG. 4. Stability analysis of the phase diagram of Eq. (3) in the (H^2, ω) parameter space at a fixed value of $E < E_c$. Region A: The homeotropic state $A = 0$ is stable. Region B: The synchronous state in which BL walls are stable. Region C: The synchronous state in which the moving Bloch walls are stable. Region D: The asynchronous state in which $\omega > \frac{\chi_a H^2}{2\gamma_1}$. The homeotropic state $A = 0$ loses stability through a pitchfork bifurcation when $H_c^2(\omega, E) > \frac{\epsilon_a(E^2 - E_c^2)}{\chi_a} + \frac{\gamma_1^2\omega^2}{\chi_a\epsilon_a(E^2 - E_c^2)}$ for $\omega < \omega_c = \frac{\epsilon_a(E^2 - E_c^2)}{\gamma_1}$ (line F_1), or a Hopf bifurcation when $H_c^2(\omega, E) > 2\frac{\epsilon_a(E^2 - E_c^2)}{\chi_a}$ for $\omega > \omega_c$ (line F_2), wall 2.

The Ising wall (BL), a heteroclinic solution which joins those two solutions, reads

$$A = \sqrt{\frac{\mu + \gamma\cos 2\delta}{a}}\tanh\left(\sqrt{\frac{\mu + \gamma\cos 2\delta}{2K_1}}x\right)e^{i\delta}.$$

It loses stability entering region C of Fig. 4 towards a moving soliton (Bloch wall) when

$$\omega > \frac{\sqrt{2\chi_a^2 H^4 + \chi_a\epsilon_a(E^2 - E_c^2)H^2 - \epsilon_a^2(E^2 - E_c^2)^2}}{3\gamma_1}. \quad (4)$$

Proceeding as in [5], we obtained that the velocity v of the Bloch wall is

$$v \sim \sqrt{K_1}\omega\frac{\sqrt{\mu - 3\sqrt{\gamma^2 - \gamma_1^2\omega^2}}}{\mu + \gamma\cos(2\delta)}. \quad (5)$$

Note that when $\gamma_1^2\omega^2 = \gamma^2$ the velocity cannot be defined since we get into the asynchronous regime in which the size of the wall diverges.

In the more realistic case when $K_1 \neq K_2$, there is no simple transformation that reduces Eq. (2) to a time independent equation like Eq. (3). The anisotropy of elasticity induces an oscillation at the core of the BL wall. This oscillation which changes the size of the wall can be understood as a continuous periodic change of splay-bend BL walls to twist BL walls. As yet understood qualitatively in [4], a more dramatic implication of the anisotropy of elasticity is to differentiate the size and the shape of the umbilics of opposite topological charge. As a consequence, in the nonequilibrium case ($\omega \neq 0$) the $+1$ and -1 umbilic selects a different wave number. This seems to be a generic feature of nonequilibrium systems for which the wave number selection mechanism is intimately related to the typical size of the vortices. We have investigated the asymmetry between the defects by placing ourselves in the parameter region corresponding to region C of Fig. 4. Numerical simulations of Eq. (2) show that a $+1$ umbilic selects a larger (smaller) wave number than a -1 umbilic when $K_2 < K_1$ (Fig. 5) (when $K_2 > K_1$). We now interpret the experimental results concerning the IB transition with a static magnetic field $\omega = 0$, $\mathbf{H} = H\hat{\mathbf{x}}$, and $\mathbf{E} = E\hat{\mathbf{z}}$. This static IB transition was introduced in [9,10] in the context of ferromagnetic systems. Analytical solutions of the BL wall, perpendicular to the magnetic field (splay-bend BL, $K = K_1, \xi = x$) or parallel to the magnetic field (twist-wall $K = K_2, \xi = y$), read

$$X = \sqrt{\mu + \gamma}\tanh\left(\xi\sqrt{\frac{\mu + \gamma}{2K}}\right), \quad Y = 0.$$

The splay-bend BL wall loses stability when $E^2 > \frac{\alpha - 1}{2\alpha\epsilon_a}\chi_a H^2 - \frac{K_3\pi^2}{\epsilon_a d^2}$ towards static Bloch wall where

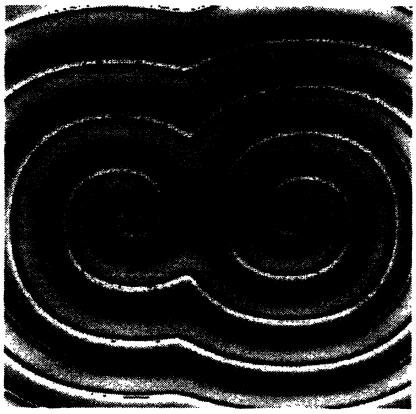

FIG. 5. Numerical simulation of Eq. (2) showing the real part of A. The asymmetry between the $+1$ and -1 spiral wave is shown by the difference of the wave number. Numerical simulations were performed in region C (Fig. 4) of the parameter space using the elastic coefficients values corresponding to MBBA at room temperature. The numerical simulations used a 256^2 grid and a finite difference method with $\delta x = 0.5$ and $\delta t = 0.005$.

$$\alpha = \frac{K_2(\sqrt{1+8K_1/K_2}-1)^2}{16K_1 - K_2(\sqrt{1+8K_1/K_2}-1)^2}.$$

The stability condition for the twist wall is obtained by interchanging K_1 and K_2 in the expression for α. The positivity of the elastic constant implies that $0 < \alpha < 1$. These predictions (Fig. 2) are in good agreement with the experimental measurement of the Ising-Bloch transition of a splay-bend BL wall. To end this Letter we remark that far from the umbilics the phase approximation leads to

$$\gamma_1 \Theta_t = K_1 \nabla^2 \Theta - \gamma \sin(2\Theta) + \gamma_1 \omega, \qquad (6)$$

where $A = Re^{i\Theta}$, $R^2 \simeq \mu + K_1(\nabla\Theta)^2 + \gamma\cos(2\Theta)$, and $K_1 = K_2$. This last equation, used in [4], gives a good approximation of the dynamics of the Bloch walls but cannot describe the spiral wave due to a phase singularity which defines the center of the spiral.

In conclusion, motivated by results [2–4,7] we have experimentally investigated the static Ising-Bloch transition and the formation of spiral waves. We related all the measurable physical quantities of the experiment in a compact which falls in good agreement with the experimental results.

* Also at URA CNRS 190, UNSA, Faculé des Sciences, 06108 Nice Cedex 2, France.

[1] W. Heflrich, Phys. Rev. Lett. **21**, 1518 (1968).
[2] L. Leger, Solid State Commun. **11**, 1499 (1972); Mol. Cryst. Liq. Cryst. **24**, 33 (1973); These d'etat, Universite Paris Sud, Orsay, France, 1976.
[3] F. Brochard, L. Leger, and R. B. Meyer, J. Phys. (Paris) Colloq. **36**, C1-209 (1975).
[4] K. B. Migler and R. B. Meyer, Phys. Rev. Lett. **66**, 1485 (1991); K. B. Migler, Ph.D. thesis, Brandeis University, Boston, MA, 1991.
[5] P. Coullet, J. Lega, B. Houchmanzadeh, and J. Lajzerowicz, Phys. Rev. Lett. **65**, 1352 (1990); P. Coullet, J. Lega, and Y. Pomeau, Europhys. Lett. **15**, 221 (1991).
[6] A. Hagberg and E. Meron, Phys. Rev. E **48**, 705 (1993).
[7] J. M. Gilli, M. Morabito, and T. Frisch, "Ising-Bloch Transition in a Nematic Liquid Crystal," J. Phys. II (France) (to be published).
[8] P. G. de Gennes, *The Physics of Liquid Crystals* (Clarendon Press, Oxford, 1974).
[9] L. N. Bulaevskii and V. L. Ginzburg, Zh. Eksp. Teor. Fiz. **45**, 772 (1963) [Sov. Phys. JETP **18**, 530 (1964)].
[10] J. Lajzerowicz and J. J. Niez, J. Phys. (Paris) Lett. **40**, L-165 (1979).

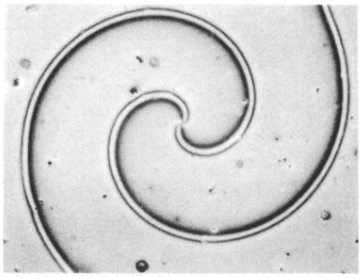

FIG. 3. Photograph of a spiral obtained with the setup of Fig. 1 in the parameter region corresponding to region C of Fig. 4.

FIG. 5. Numerical simulation of Eq. (2) showing the real part of A. The asymmetry between the $+1$ and -1 spiral wave is shown by the difference of the wave number. Numerical simulations were performed in region C (Fig. 4) of the parameter space using the elastic coefficients values corresponding to MBBA at room temperature. The numerical simulations used a 256^2 grid and a finite difference method with $\delta x = 0.5$ and $\delta t = 0.005$.